

# Passive and Active Coupling Comparison of Fuel Cell and Supercapacitor for a Three-Wheel Electric Vehicle

A. Macias<sup>1\*</sup>, M. Kandidayeni<sup>1</sup>, L. Boulon<sup>1,2</sup>, J. Trovão<sup>3,4</sup>

<sup>1</sup> Université du Québec à Trois-Rivières, Hydrogen Research Institute, Trois-Rivières, QC, Canada

<sup>2</sup> Canada Research Chair in Energy Sources for the Vehicles of the Future

<sup>3</sup> e-TESC Laboratory, Dept. Electrical & Computer Engineering, University of Sherbrooke, Sherbrooke, QC, J1K 2R1, Canada

<sup>4</sup> Canada Research Chair in Efficient Electric Vehicles with Hybridized Energy Storage Systems

*[\*]Corresponding author: [alvaro.omar.macias.fernandez@uqtr.ca](mailto:alvaro.omar.macias.fernandez@uqtr.ca)*

## **Abstract**

The desire to reduce the power electronics related issues has turned the attentions to passive coupling of powertrain components in fuel cell hybrid electric vehicles (FCHEVs). In the passive coupling, the fuel cell (FC) stack is directly connected to an energy storage system on the DC bus as opposed to the active configuration where a DC-DC converter couples the FC stack to the DC bus. This paper compares the use of passive and active couplings in a three-wheel FCHEV to reveal their strengths and weaknesses. In this respect, a passive configuration, using a FC stack and a supercapacitor, is suggested first through formulating a sizing problem. Subsequently, the components are connected in an active configuration where an optimized fuzzy energy management strategy is used to split the power between the components. The performance of the vehicle is compared at each case in terms of capital cost and trip cost, which is composed of FC degradation and hydrogen consumption, and total cost of the system per hour. The obtained results show the superior performance of the passive configuration by 17% in terms of total hourly cost, while the active one only results in less degradation rate in the FC system.

**Keywords:** Active Configuration, Electric Vehicles, Fuel Cell, Hybridization, Hydrogen Car, Passive Coupling, Supercapacitor, Ultracapacitor.

## 1 Introduction

Conventional vehicles powered by fossil fuels are considered as major contributors to air pollution and have made transportation one of the main responsible sectors for CO<sub>2</sub> emissions [1]. While the air pollution poses considerable risks for human health and environment, its harmful effects can be mitigated through electrification of transport systems [2]. Among the existing technologies, such as electric vehicles, hybrid electric vehicles etc., FC vehicle is one of the most auspicious due to zero-local emissions, high level of driving autonomy, and fast refueling time [3]. However, FC systems cannot tolerate sudden and significant fluctuations in the load which are normal in vehicular applications [4]. The load peaks can cause air/fuel starvation in the FC system resulting in serious power drop [5, 6]. Furthermore, abrupt changes in the load have detrimental effects on the lifetime of the FC stack since it accelerates the degradation rate of the system [7, 8]. Hybridization of a FC system with other sources, such as batteries and supercapacitors (SCs), has been widely used in the literature to alleviate the problems regarding the slow dynamic essence of a FC system [9]. The main goal of this hybridization is to supply the power peaks with an energy storage device and benefit from the regenerative braking mechanism. Different hybridization configurations can be found in the literature [10-13]. In [12], a review of six topologies, which can be mainly fallen into two categories of active and passive, for a FCHEV is presented. Active configuration refers to the connection of the power source to the DC bus via a converter. In active configurations, normally, an energy management strategy (EMS) is required to perform the power split among the components while satisfying the requested power. Several EMSs from rule based and optimization based to intelligent based strategies have been proposed for such configuration [14]. Among them, fuzzy logic control (FLC) is one of the most commonly used due to the flexibility, robustness, and convenient implementation [15]. FLCs provide strategic rules by using linguistic labels. Several grounds, such as inaccurate model of a vehicle's components, nonlinearity, and unknown aspects, like traffic, weather, etc., can be

mentioned for appropriateness of employing a FLC in FCHEV application. Contrary to the active configuration, passive coupling refers to the connection of the component directly to the DC bus. This kind of architecture is independent of an EMS and has self-management due to the characteristics (different impedance) of the components. The passive configuration provides similar benefits as the active architecture while it does not require any DC-DC converter saving of weight, cost, and energy losses linked with an extra level of power conversion. However, the drawback of the passive hybrid system is that the FC stack is the main responsible for supplying the requested traction power as there is no controlled power regulation among the power sources. The power split between the FC system and the SCs depends on the natural behavior of each source (internal resistor and open circuit voltage for instance). Therefore, several authors refer to it as “natural energy management” [16, 17]. This can lead to the presence of higher power ripples at the FC side and consequently increase the degradation rate of the stack. In [10], the comparison of active and passive hybrid configurations of FC and battery, as an auxiliary power unit of trucks, reveals that the direct coupling of FC and battery has a better performance as long as the demanded power does not have substantial variations. However, marked fluctuations of the demanded power can make the FC operate in low-efficiency regions. The selection of active and passive configurations has been considered in a FCHEV, using a SC bank and a battery pack as the secondary power source units [11]. This study demonstrates that the active coupling of the battery with the FC stack leads to high power variations in the stack while the passive connection of FC-SC makes the requested power from the FC smoother and has a higher energetic efficiency. Although active configuration provides a better management of the components, several researchers have opted to use passive connections to reduce the complexity, cost, and weight of the system [18]. In this among, the direct connection of FC with SC, as an energy storage system, is more prevalent, compared to the battery, due to the capability of a SC in coping with intermittency of behavior in FCHEV applications. In [19-21], the main focus is on the

direct hybridization of SC to a single FC. The obtained experimental results indicate that the passive connection avoids negative voltage, provides self-protection against sudden power changes, increases the dynamic of the system, and enhances the electrical performance as patented by NISSAN company [22]. In [23], the performed study takes the arrangement of SCs into consideration in the passive configuration and concludes that increasing the number of SCs reduces the power supplied by the FC as well as the hydrogen consumption, while escalating the capital cost of the system. In [24, 25], the FC-SC passive coupling is specifically used for the vehicular application. In [26], the simulation results show that the direct hybridization of FC-SC benefits from high fuel economy and recovers more regenerative energy than battery due to its low internal resistance. In [27], the experimental results of a 9.5-kW proton exchange membrane FC (PEMFC) passively coupled with a SC array illustrate a reduction in dynamic load, idling time, and rapid load changes in the FC without using a DC/DC converter.

In the light of the discussed manuscripts, it is obvious that some attempts have been already done regarding the direct coupling of FC and SC in vehicular applications. However, such a coupling has never been used for a recreational three-wheel electric vehicle so far. These types of vehicles are normally exposed to high dynamics and need to be light and compact. The thing that makes the choice of passive couplings interesting here is that these configurations provide low mass and compactness through the elimination of power electronics. Moreover, SC, which is a prevalent component in this kind of configuration, is highly capable of dealing with high dynamics. In this regard, a comparative analysis of FC-SC passive and active configurations for a three-wheel vehicle, which has more power demand variation than conventional vehicles, is put forward in this manuscript. To do so, firstly, the minimum required size of the main components is determined in order to meet the requested power since this type of vehicle is expected to have low mass and volume. Afterwards, the performance of the three-wheel electric vehicle is assessed by using the

selected components in both of passive and active configurations. Passive configuration benefits from self-management and does not require the design of an EMS. However, in the active configuration, the power split is performed by using an optimized fuzzy strategy. As opposed to other similar works which only use the hydrogen consumption as a means of comparison, a detailed performance index based on capital cost and trip cost of the system is defined in this work. Moreover, a real driving cycle from the three-wheel electric vehicle is utilized to carry out the simulation.

The remainder of this paper is organized as follows. The vehicle modeling with passive and active configurations is described in Section 2. The designed EMS for the active configuration is presented in Section 3. The obtained results of the comparative analysis are discussed in Section 4. Finally, the conclusion is given in Section 5.

## **2 Modeling**

### **2.1 Components sizing**

The studied vehicle in this paper (e-TESC-3W platform shown in Figure 1) is a three-wheel electric vehicle used essentially for leisure purposes. This prototype is currently used as a test bench at e-TESC laboratory of University of Sherbrooke [28]. The e-TESC-3W platform has a 28-kW (96 V) permanent magnet synchronous motor (PMSM) directly connected to the rear wheel. The main specifications of this vehicle are listed in Table 1 and explained thoroughly in [28]. This vehicle can reach a maximum speed of 120 km h<sup>-1</sup>.



Figure 1: The studied e-TESC 3W vehicle

Table 1: Vehicle specifications

Variable	Symbol	Value	Units
Vehicle mass (w/o power source)	$M_{eq}$	350	kg
Typical rolling resistance coefficient	$\mu_{fr}$	0.02	-
Typical aerodynamic drag coefficient	$C_D$	0.75	-
Vehicle front area	$A_f$	1.25	m <sup>2</sup>
Wheel radius	$r$	0.305	m
Belt transmission drive ratio	$G_{gb}$	5.033 (30:151)	-
Belt transmission drive efficiency	$\eta_{gb}$	95	%
Maximum speed	$V_{max}$	120	km h <sup>-1</sup>
Acceleration speed	$V_{acc}$	100	km h <sup>-1</sup>
Acceleration time	$t_{acc}$	7	s
Grade slope at 100 km/h	$\theta$	0.03	%

Originally, e-TESC-3W platform has been a pure battery electric vehicle (BEV). In [29], a coupling of battery, as the main power source, and the SC, as the energy storage system, is proposed for this vehicle where battery supplies the average power while the SC is held responsible for the high dynamic phase. The authors in [29] indicate that their proposed hybrid configuration can enhance the lifetime of the e-TESC 3W platform powertrain components compared to the pure BEV. The principal objective of the current manuscript is to provide a comparison of passive and active FC-SC powertrain configurations for the e-TESC 3W platform. To do so, initially, performing a component sizing to figure out the rated power of the FC and SC in relation to the requirements of the vehicle is necessary. Leisure activity vehicles are typically characterized as being light and compact, but with a high acceleration and speed capabilities. In this regard, the sizing problem should ascertain the minimum required component dimensions to satisfy the requested power for all the constraints specified in Table 2 [30].

Table 2: FC stack and SC characteristics

Component	Parameter	Variable	Value	Units
FC	No. cells	$N_{cell}$	135	Cells
	Max power	$P_{FC,max}$	27.3	kW
	Max current	$i_{FC,max}$	300	A
	OCV voltage	$V_{FC,OCV}$	130.2	V
	Max temperature	$T_{FC,max}$	70	°C
	Thermal capacity	$MC_{fc}$	140	kJ K <sup>-1</sup>
	Power of fan	$P_{fan}$	200	W

	Stack mass	FC <sub>mass</sub>	19.5	kg
	Current slew rate	FC <sub>SR</sub>	20	As <sup>-1</sup>
SC	No. SC in series	SC <sub>serie</sub>	50	
	SC mass	SC <sub>mass</sub>	510	gr
	Equivalent series resistance (ESR)	SC <sub>ESR</sub>	0.29	mΩ
	Capacitance	SC <sub>c</sub>	3000	F
	Rated voltage	SC <sub>v, rated</sub>	2.7	V
	Max current	SC <sub>Max, i</sub>	1900	A
	Cut-off frequency	SC <sub>cut-off</sub>	26	mHz

Based on the specifications, the FC needs to be sized in a way to supply the maximum power for a long distance, continuous, and high-speed driving. Otherwise the SC will get discharged quickly [31]. The FC supplies the base power ( $P_e$ ) in the maximum speed condition premised on the hybrid vehicle traction force resistance ( $F_{env}$ ) as:

$$P_e = F_{env} V_{EV} / (1000 \eta_t \eta_{em}) \quad (1)$$

$$F_{env} = F_{roll} + F_{grade} + F_{air} \quad (2)$$

$$F_{roll} = M_{eq} g \mu_{fr} \cos(\theta) \quad (3)$$

$$F_{air} = 0.5 \rho_a A_f C_d V_{EV}^2 \quad (4)$$

$$F_{grade} = M_{eq} g \sin(\theta) \quad (6)$$

where  $F_{roll}$  is the rolling resistance force,  $F_{grade}$  is the grade related force,  $F_{air}$  is the resistance force against the air,  $M_{eq}$  is the mass of the vehicle,  $g$  is gravity,  $\mu_{fr}$  is the rolling resistance coefficient,  $\rho_a$  is the air density,  $C_d$  is the aerodynamic drag coefficient,  $A_f$  is the frontal area,  $V_{EV}$  is the vehicle speed,  $\theta$  is the road grade,  $\eta_t$  is the transmission efficiency, and  $\eta_{em}$  is the motor average efficiency [32]. Solving Eq. (1) leads to the value of 26.5 kW for  $P_e$  under maximum speed condition (120 km h<sup>-1</sup>) on a flat road. This value defines the size of the FC for steady conditions. Moreover, the maximum electric power for the vehicle acceleration from 0 to 120 km h<sup>-1</sup> in 7 seconds comes to 88 kW on a flat road, obtained by:



$$P_{\text{tot}} = (F_{\text{roll}} + F_{\text{grade}} + F_{\text{air}} + F_{\text{acc}}) V_{\text{EV}} / (1000 \eta_t \eta_{\text{em}}) \quad (7)$$

$$F_{\text{acc}} = M_{\text{eq}} \delta d V_{\text{EV}} / dt \quad (8)$$

where  $F_{\text{acc}}$  is the accelerating force, and  $\delta$  is the mass factor related to the rotational inertia.  $\delta$  is assumed to be 1.035 for a one-speed gear-box [33].

With respect to the calculated  $P_{\text{tot}}$ , the minimum SC size should be 60.7 kW while the selected FC size is 27.3 kW (FCvelocity-9SSL) from Ballard [34, 35]. The utilized SC in this work is K2 Series from Maxwell Technologies [24]. The characteristics of the selected components are listed in Table 2.

It is worth reminding that due to the direct connection of the SC bank and FC stack in passive configuration, the SC nominal voltage needs to be higher than the open circuit voltage of the FC. In this respect, the studied system requires 50 SCs connected in series. Regarding the active configuration, a 30-kW DC/DC converter (non-isolated) with a mass around 11 kg is used [36].

The tank size selection is done by assuming a similar autonomy as the pure electric e-TESSC 3W platform, which is around 150 km for a full charge. Taking into account this autonomy and the performance of the FC system in the lowest efficient zone, which is at the maximum speed of 120 km h<sup>-1</sup>, the required hydrogen would be 1.77 kg. Based on the targets of light-duty fuel cell vehicles of DOE, the system volumetric capacity of the tank in 2020 should be 0.040 kg H<sub>2</sub> L<sup>-1</sup> [37]. Therefore, the weight of the high-pressure tank in this manuscript comes to 32.2 kg.

## 2.2 Energetic Macroscopic Representation

In this manuscript, energetic macroscopic representation (EMR), which is a graphical method to organize the model of complex multiphysics systems, is used to model the e-TESSC 3W platform in both active and passive configurations [38, 39]. The traction system of e-

TESC 3W platform vehicle is shown in Figure 2. Passive and active energy source subsystems (ESSs) are presented in Figure 3 and Figure 4 respectively. According to Figure 2, the hybrid vehicle velocity can be derived from the traction force and traction force resistance as [28]:

$$M_{eq} dV_{EV}/dt = F_{tr} - F_{env} \quad (9)$$

$$F_{tr} = (G_{gb}/r) T_{em} \eta_{gb}^{\zeta} \quad (10)$$

$$\Omega_m = (G_{gb}/r) V_{EV} \quad (11)$$

$$\zeta = 1, \text{ for } T_{em} \geq 0 \quad (12)$$

$$\zeta = -1, \text{ for } T_{em} < 0 \quad (13)$$

$$T_{em} = T_{em\_r} \quad (14)$$

where  $F_{tr}$  is the traction force,  $G_{gb}$  is the gearbox transmission ratio,  $r$  is the wheel radius,  $T_{em}$  is the electric machine torque,  $\eta_{gb}$  is the Gearbox transmission efficiency,  $\Omega_m$  is the rotor rotation speed, and  $T_{em\_r}$  is a reference torque to control the electric machine.

The requested current of the vehicle from the electric motor side ( $i_{ts}$ ) is then formulated as:

$$i_{ts} = (T_{em} \Omega_m \eta_m^{\beta})/U_{SC} \quad (15)$$

where  $U_{SC}$  is the SC voltage. In the passive configuration, as it can be seen in Figure 3, there is no DC-DC converter and a diode is used in series with the PEMFC stack to prevent the reversed current.

The equivalent resistor of the diode ( $r_D$ ) along with the voltage difference of the FC ( $U_{fc}$ ) and SC ( $U_{SC}$ ) determine the current of the FC system ( $i_{FC-sys}$ ).

$$i_{FC-sys} = (U_{fc} - U_{SC})/r_D \quad (16)$$

$$\dot{i}_{ts} = \dot{i}_{FC\text{-sys}} + \dot{i}_{SC} \quad (17)$$

where  $i_{SC}$  is the current of the SC. On the other hand, in the active configuration, as shown in Figure 4, the current goes through a converter as [36]:

$$\dot{i}_{FC\text{-sys}} V_{fc} = \dot{i}_{dc/dc} U_{SC} \eta_{dc/dc} \quad (18)$$

$$\dot{i}_{ts} = \dot{i}_{dc/dc} + \dot{i}_{SC} \quad (19)$$

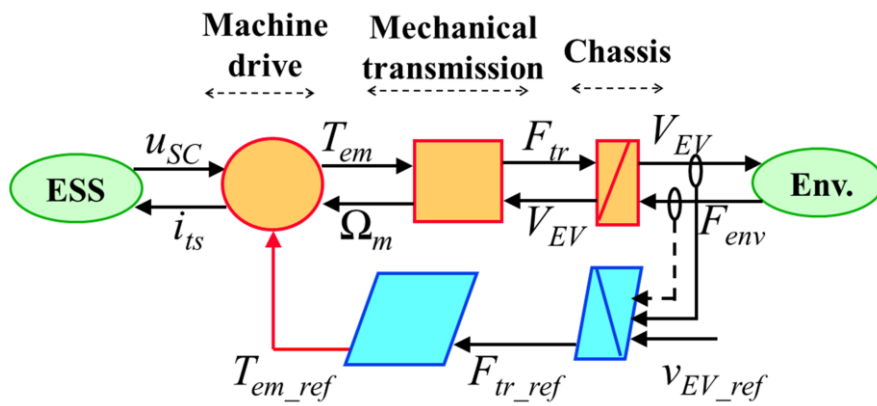


Figure 2: Traction system of the e-TESS 3W platform vehicle

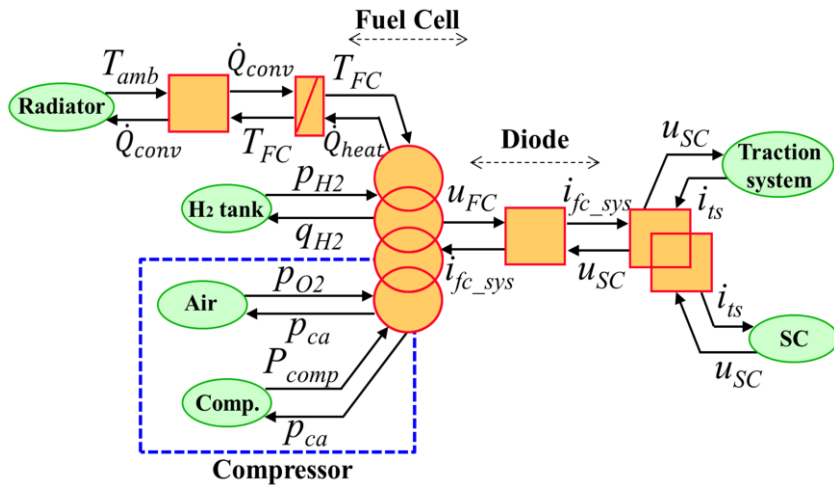


Figure 3: The proposed passive ESS for the e-TESS 3W platform vehicle

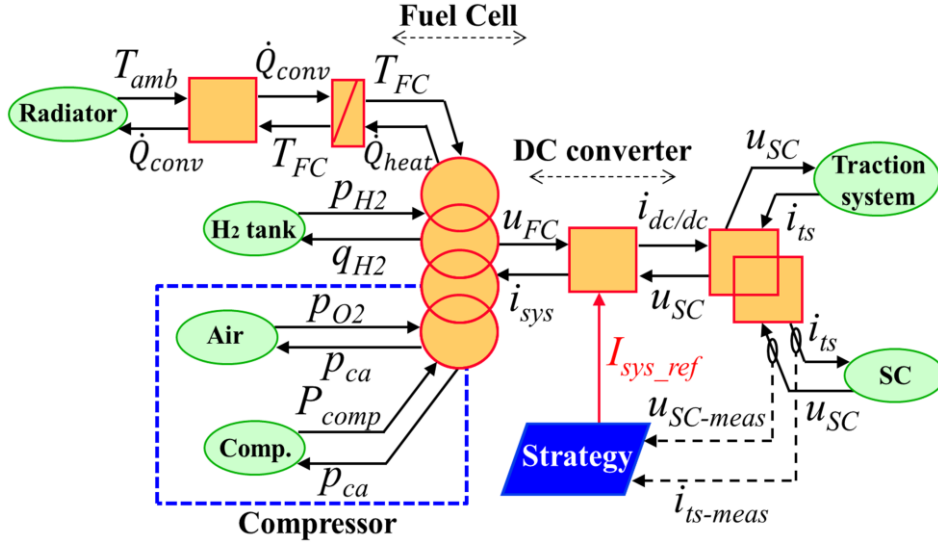


Figure 4: The utilized active ESS of e-TESS 3W platform vehicle

where  $i_{dc/dc}$  is the converter current and  $\eta_{dc/dc}$  is the converter efficiency.

The PEMFC voltage ( $U_{fc}$ ) is calculated by using the semi-empirical model suggested in [40].

$$U_{fc} = N_{cell} \times (E_{Nernst} + U_{act} + U_{ohmic} + U_{con}) \quad (20)$$

$$E_{Nernst} = 1.229 - 0.85 \times 10^{-3} (T_{fc} - 298.15) + 4.3085 \times 10^{-5} T_{fc} [\ln(p_{H2}) + 0.5 \ln(p_{O2})] \quad (21)$$

$$U_{act} = Y_1 + Y_2 T_{fc} + Y_3 T_{fc} \ln(CO_2) + Y_4 T_{fc} \ln(i_{FC}) \quad (22)$$

$$CO_2 = p_{O2} / 5.08 \times 10^6 e^{-(498/T_{fc})} \quad (23)$$

$$U_{ohmic} = -i_{FC} R_{internal} = -i_{FC} (\xi_1 + \xi_2 T_{fc} + \xi_3 i_{FC}) \quad (24)$$

$$U_{con} = \alpha i_{FC}^G \ln(1 - \beta i_{FC}) \quad (25)$$

where  $E_{Nernst}$  is the reversible voltage,  $U_{act}$  is the activation loss,  $U_{ohmic}$  is the ohmic loss,  $U_{con}$  is the concentration loss,  $T_{fc}$  is the stack temperature,  $p_{H2}$  is the hydrogen partial pressure,  $p_{O2}$  is the oxygen partial pressure,  $Y_n$  ( $n = 1 \dots 4$ ) is the empirical coefficients,  $CO_2$  is the oxygen concentration,  $i_{fc}$  is the the FC operating current,  $R_{internal}$  is the internal resistor defined by the three parametric coefficients  $\xi_n$  ( $n = 1 \dots 3$ ),  $\alpha$  is a semi-empirical parameter related to the

diffusion mechanism ( $0.3 \leq \alpha \leq 1.8$ ),  $G$  is a dimensionless number related to the water flooding phenomena ( $1 \leq G \leq 4$ ), and  $\beta$  is the inverse of the limiting current.

The thermal behavior of the stack is modeled by using the energy conservation law. The energy balance for describing the temperature dynamic of the PEMFC can be given by [41]:

$$Q_{\text{heat}} = N_{\text{fc}} i_{\text{fc}} (1.254 - U_{\text{fc}}) \quad (26)$$

$$H_{\text{fc}} = (N_{\text{fc}}/36)(2700k_{t1} + k_{t2}) \quad (27)$$

$$Q_{\text{conv}} = H_{\text{fc}}(T_{\text{fc}} - T_{\text{amb}}) \quad (28)$$

$$dT_{\text{fc}}/dt = (Q_{\text{heat}} - Q_{\text{conv}})/MC_{\text{fc}} \quad (29)$$

where  $Q_{\text{heat}}$  is the generated heat in the FC,  $N_{\text{fc}}$  is the number of cells,  $H_{\text{fc}}$  is the heat transfer coefficient,  $k_{t1}$  and  $k_{t2}$  are the coefficients obtained experimentally in [41],  $T_{\text{amb}}$  is the ambient temperature,  $T_{\text{fc}}$  is the stack temperature,  $Q_{\text{conv}}$  is the convection heat transfer, and  $MC_{\text{fc}}$  is the thermal capacity of the FC.

The current of the PEMFC system ( $i_{\text{FC-sys}}$ ) is obtained by considering the losses from the balance of plant as [41, 42]:

$$i_{\text{FC-sys}} = (P_{\text{fc}} - P_{\text{comp}} - P_{\text{fan}})/U_{\text{fc}} \quad (30)$$

$$P_{\text{comp}} = \eta_{\text{comp}}^{-1} W_{\text{air}} c_p T_{\text{amb}} ((p_{\text{ca}}/p_{\text{amb}})^{(\gamma-1)/\gamma} - 1) \quad (31)$$

$$P_{\text{fc}} = U_{\text{fc}} i_{\text{fc}} \quad (32)$$

$$W_{\text{air}} = \lambda W_{\text{O}_2}/\chi_{\text{O}_2} \quad (33)$$

$$W_{\text{O}_2} = M_{\text{O}_2} N_{\text{fc}} i_{\text{fc}}/2F \quad (34)$$

$$p_{\text{O}_2} = 0.21p_{\text{ca}} \quad (35)$$

$$p_{\text{H}_2} = 0.99p_{\text{an}} \quad (36)$$

$$p_{\text{ca}} = a_1 + a_2 i_{\text{fc}} + a_3 i_{\text{fc}}^2 + a_4 i_{\text{fc}}^3 \quad (37)$$

$$p_{\text{an}} = p_{\text{ca}} + 20000 \quad (38)$$

where  $P_{\text{comp}}$  is the consumed power by the compressor,  $p_{\text{ca}}$  is the pressure in the cathode,  $P_{\text{fan}}$  is the consumed power by the FC fan (200 W),  $\eta_{\text{comp}}$  is considered as the average compressor efficiency (0.70) [43],  $W_{\text{air}}$  is the rate of used air,  $c_p$  is the air specific heat capacity ( $1005 \text{ JK}^{-1}$ ),  $p_{\text{amb}}$  is the ambient pressure,  $\gamma$  is the ratio of specific heats of air (1.4),  $\lambda$  is the oxygen excess ratio which is two,  $W_{\text{O}_2}$  is the oxygen consumption rate,  $\chi_{\text{O}_2}$  is the oxygen mass fraction (0.233),  $M_{\text{O}_2}$  is oxygen molar mass,  $F$  is the Faraday constant,  $p_{\text{an}}$  is the pressure in the anode, and  $a_i (i=1 \dots 3)$  is the experimentally obtained coefficient.

The hydrogen flow ( $q_{\text{H}_2}$ ) is calculated based on an experimental formula as [34]:

$$q_{\text{H}_2} = 0.00696 i_{\text{fc}} N_{\text{fc}} \quad (39)$$

Based on the mentioned models, the efficiency of the FC system is calculated considering the power losses of the auxiliaries:

$$\eta_{\text{sys}} = (P_{\text{fc}} - P_{\text{comp}} - P_{\text{fan}}) / (q_{\text{H}_2} \text{ HHV}) \quad (40)$$

where the generated hydrogen power is the product of hydrogen flow and the high heating value of hydrogen ( $\text{HHV} = 286 \text{ kJ mol}^{-1}$ ). In the active coupling, the converter efficiency is multiplied by the FC system efficiency to know the efficiency in the DC bus.

Finally, the SC is modeled based on the equivalent circuit proposed in [44].

$$U_{\text{SC}} = r_{\text{SC}} i_{\text{SC}} + (1/C_{\text{SC}}) \int i_{\text{SC}} dt \quad (41)$$

where  $r_{\text{SC}}$  is the SC bank resistance and  $C_{\text{SC}}$  is the SC bank capacitance.

### 2.3 Degradation

One of the most significant factors while using a FC system as the main power source of a vehicle is durability consideration. This is mainly due to the fact that FC is really damage prone although it is one of the costly components of the powertrain. In automotive applications, the end of life (EOL) of a FC stack is defined when a 10% voltage loss is reached [45]. For this reason, it is vital to include the degradation of the FC stack in the analysis of the system performance. According to [25, 46, 47], the causes of FC degradation fit into five cases of load changing, startup and shutdown, low power load (idle condition), high power load, and natural decay. An empirical model for determining the voltage degradation of the FC stack can be formulated as [46]:

$$\Delta FC_{deg} = \Delta FC_{nat} + \Delta FC_{add} \quad (42)$$

where  $\Delta FC_{deg}$  denotes the degradation of the FC in percentage,  $\Delta FC_{nat}$  is the natural decay rate related to the expected lifetime of the FC in normal operation conditions, and  $\Delta FC_{add}$  is the degradations rooted from unfavourable operations.

The influence of each factor on the degradation of the FC can be defined as:

$$\Delta FC_{deg} = k_1 t_1 + k_2 n_1 + k_3 t_2 + k_4 t_3 + \beta_{nat} t_{FC\_ON} \quad (43)$$

where  $t_1$  is the idle time,  $n_1$  is the number of start-stops,  $t_2$  is the duration of heavy loading, and  $t_3$  is the time in high power condition. The idle condition is described as the output power which is less than 5% of maximum power ( $P_{Low}$ ), the heavy loading is an absolute variation more than 10% of maximum power per second, and high power is delimited as higher than 90% of maximum power ( $P_{High}$ ). Based on the 2020 FC lifetime target of DOE (5000 hours), the natural decay rate  $\beta_{nat}$  is set to reach a voltage loss of 10% in 5000 hours [48]. Table 3 represents all the degradation rates for all the phenomena based on experimental data [25].

In addition to the FC stack, a calendar degradation model has been considered for the SC based on the datasheet of the manufacturer. According to this datasheet, the expected lifetime of this device is 10 years. Moreover, the EOL of the SOC is defined as an increment of 100% in  $SC_{ESR}$  and a decrement of 20% in  $SC_C$  [24].

Table 3: FC degradation coefficients

Coefficient	Value	Units
$k_1$	0.00126	% h <sup>-1</sup>
$k_2$	0.00196	% per cycle
$k_3$	0.0000593	% h <sup>-1</sup>
$k_4$	0.00147	% h <sup>-1</sup>
$\beta$	0.002	% h <sup>-1</sup>

### 3 Energy management strategy for active coupling

As explained earlier, the main purpose of this work is to compare the use of FC-SC passive and active couplings for the e-TESS 3W platform vehicle. Passive configuration does not need an EMS as the operating current harmonics are chiefly provided by the component with the lowest impedance, SC herein, in such configuration. However, to bring into attention the strengths of the utilized passive architecture, its performance is compared with an active configuration where the same selected FC stack is connected to the DC bus through a DC-DC converter and the SC is directly connected to the bus. Such active configuration needs an EMS to split the power between the FC and SC. In this respect, a FLC based EMS is designed and optimized by genetic algorithm (GA) for the purpose of this paper. FLC uses some if-then rules to integrate the knowledge of an expert into the design procedure and does not require a precise model of the system. Since the comparative analysis of this work is mainly based on a specific real deriving cycle, the parameters of the FLC has been adjusted by GA to improve its performance as much as possible for this known driving cycle.

The designed FLC for the purpose of power splitting in the active powertrain of this work has two inputs, requested power and SC voltage, and one output, which is the required power from the FC. The input and output membership functions (MFs) of the FLC as well as the



fuzzy reasoning rules are tuned by GA. Since the optimization of FLC is a common approach in the literature [49, 50], its explanation has been considered unnecessary in this manuscript. The proposed cost function for optimizing the performance of the FLC is as follows.

$$C_{\text{Trip}} = FC_{\text{cost}} \Delta_{\text{FC}} + H_{2,\text{cost}} H_{\text{cons}} \quad (44)$$

where  $FC_{\text{cost}}$  is the cost of the FC, specified in Table 4,  $\Delta_{\text{FC}}$  is the degradation percentage of the FC, obtained by Eq. (43),  $H_{2,\text{cost}}$  is the cost per kilogram of hydrogen, and  $H_{\text{cons}}$  is the hydrogen consumed during the trip. Table 4 shows the cost breakdown of the complete power source system.

Table 4: Coefficient for FC degradation model

Component	Cost	Reference
Storage system	\$ 589.5	[37]
$FC_{\text{cost}}$	\$ 1092	[48]
$H_{2,\text{cost}}$	\$ 2.3 per kg	[51]
SC	\$ 1965	[52]
DC/DC converter	\$ 1500	[53]

Figure 5 shows the comparison of the FC system efficiency between active and passive configurations. According to this figure, the overall efficiency of the passive system is higher than the active system due to the exclusion of the power electronic related losses. Figure 5 also delimits the low power ( $P_{\text{Low}}$ ) zone, which is 5% of the maximum power, and high power ( $P_{\text{High}}$ ) zone, which is 90% of the maximum power. For both cases of passive and active configurations, the maximum efficiency is located near to  $P_{\text{Low}}$ .

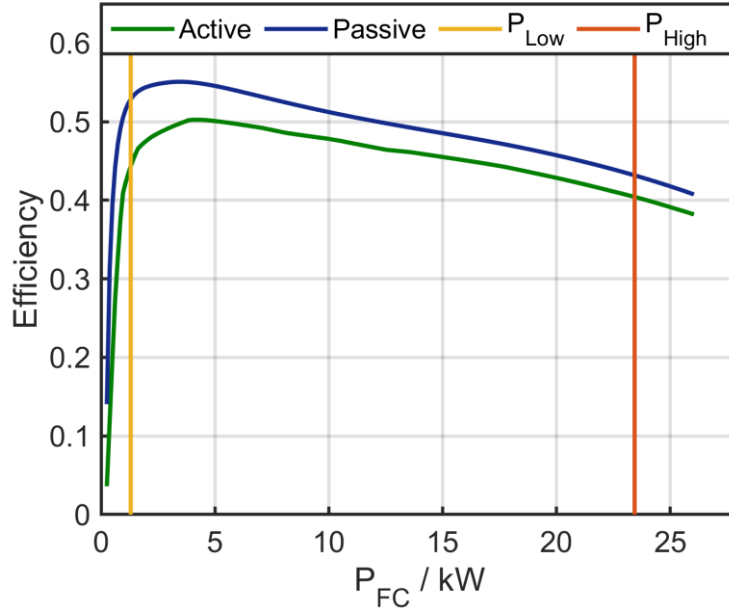


Figure 5: FC system efficiency comparison of active and passive couplings

The optimization process has been carried out for a real driving cycle recorded from e-TESSC 3W platform shown in Figure 6. The optimized reasoning rules of the FLC are presented in Figure 7. From this figure, it is clear that the optimized EMS avoids unnecessary on-off cycles. Indeed, it keeps the FC stack in a very low (VL) power mode when the requested power is low, and the voltage of the SC is high. Moreover, the FC stack tries to maintain the SC voltage in high levels in order to embrace any sudden peaks of power. Figure 8 shows the initial and optimized MFs of the two inputs and one output. Regarding the MFs of the first input ( $P_{ts}$ ) and the output ( $I_{FC}$ ), it can be seen that they have almost formed an equal distribution over the universe of discourse. On the contrary, in the second input ( $U_{SC}$ ), the low level covers up to 40% of the range of value. This range implies that the optimization algorithm has opted to keep the SC within a high level of energy to deal with the high dynamics behavior of the profile. In order to clarify the obtained shape in the MFs of the optimized fuzzy, it should be reminded that a trapezoidal MF can be defined as Trapezoidal ( $x; a, b, c, d$ , while  $a < b < c < d$ ):

$$0 \quad x < a \quad (45)$$

$$m_1 = x-a/b-a \quad a \leq x \leq b \quad (46)$$

$$1 \quad b \leq x \leq c \quad (47)$$

$$m_2 = d-x/d-c \quad c \leq x \leq d \quad (48)$$

$$0 \quad d \leq x \quad (49)$$

where  $x$  represents real value (Crisp Value) within the universe of discourse while  $a, b, c, d$  represent a  $x$ -coordinates of the four heads of the trapezoidal. During the optimization process of this work, the two constructing slopes of each trapezoidal MF ( $m_1$  and  $m_2$ ) has been forced to reach the same value.

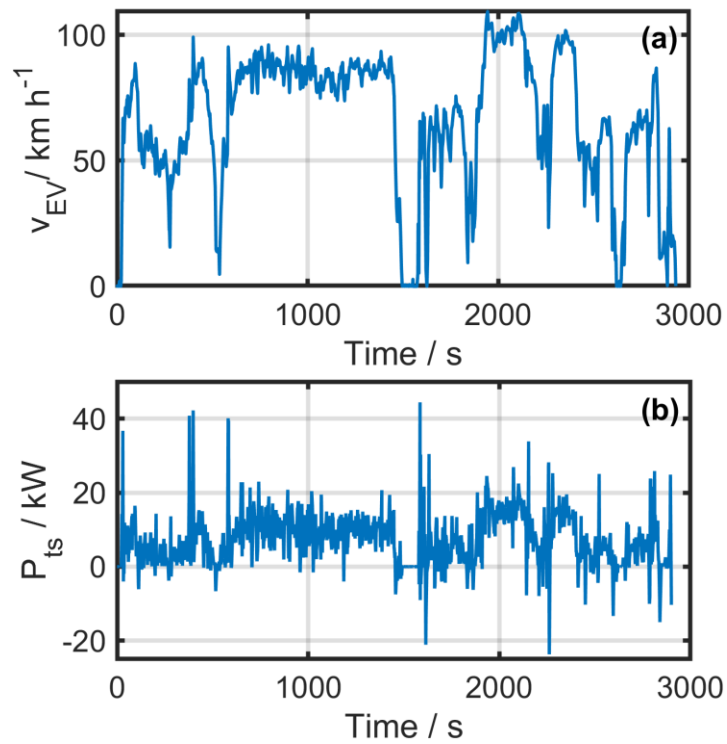


Figure 6: The real driving cycle of e-TESS 3W platform vehicle

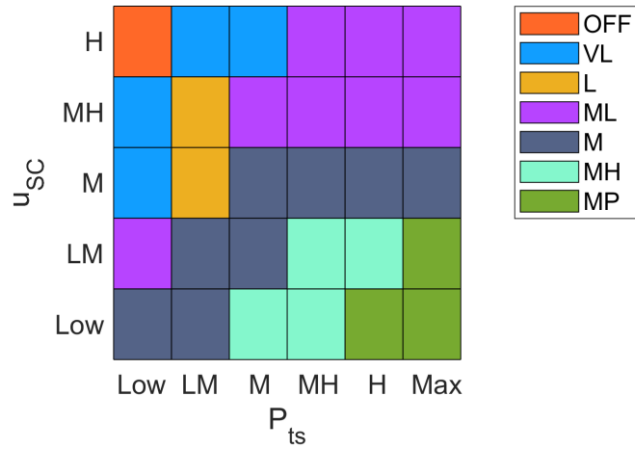


Figure 7: Optimized rules of FLC

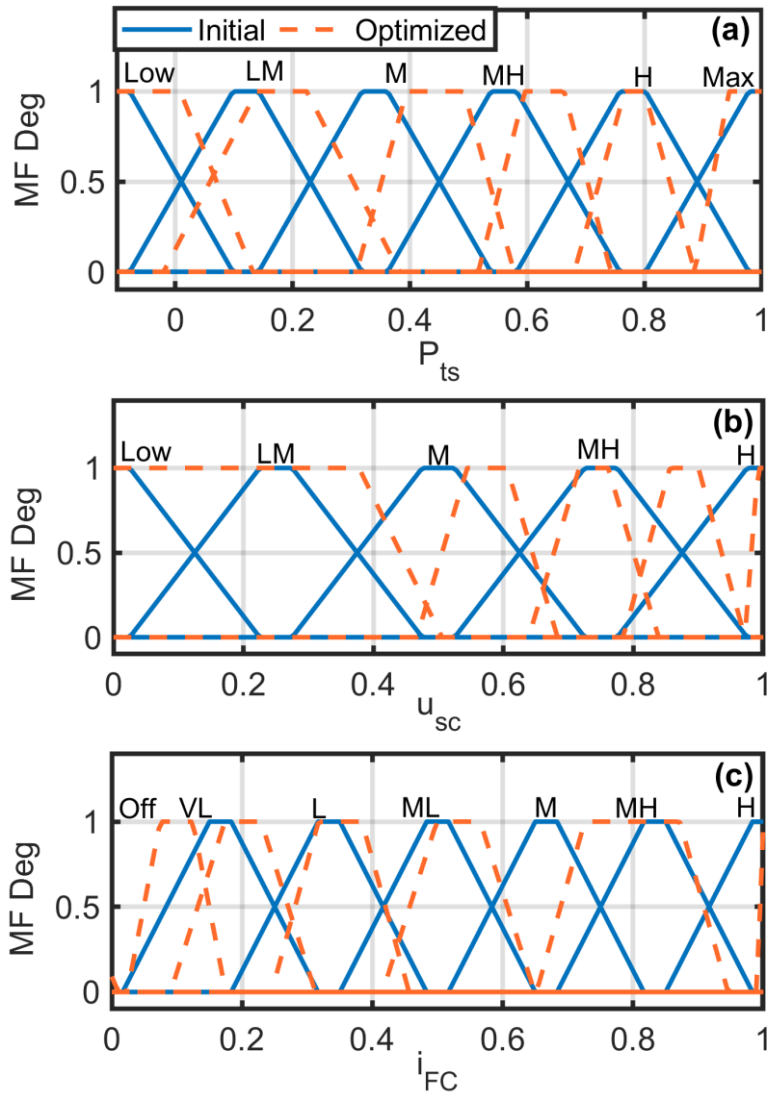


Figure 8: Optimized FLC MFs, a) requested power (input 1), b) voltage of SC (input 2), and c) required current from the FC (output)

#### 4 Results and discussion

The achieved results of the carried out comparative study is presented in this section.

Primarily, the results related to the split and distribution of the power among the power sources are investigated. Secondly, the cost of FC degradation and hydrogen consumption are compared for each of the configurations. Finally, other aspects, such as the trip cost, total cost of the system, and hourly system cost, are compared for each case study.

Figure 9 shows the power split between the FC stack and SC bank in each configuration.

Comparison of the active and passive configurations shows that in the active coupling, the SC operates in a wider range which leads to the high efficiency performance of the FC stack.

Regarding the passive coupling, it is clear that the extracted power from the FC stack follows a smoother path since the SC bank functions as a low-pass filter in such configurations. It is worth mentioning that both of the passive and active configurations respect the current slew rate of the FC specified in Table 2.

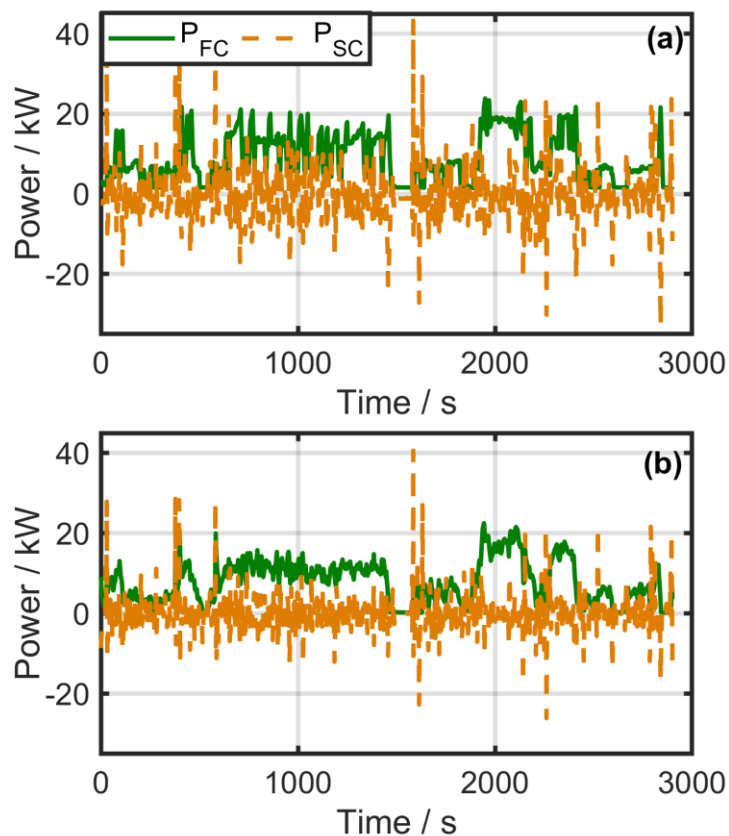


Figure 9: Power split signals for a) active and b) passive configuration

From Figure 10, it can be seen that active configuration manages to run the FC stack between  $P_{Low}$  and  $P_{High}$  regions. Operating the FC stack within this region results in higher efficiency and less degradation of the system. Figure 10b shows that the passive configuration provides a homogeneous power distribution while it sometimes leads to the operation of the FC system in the low efficiency zone.

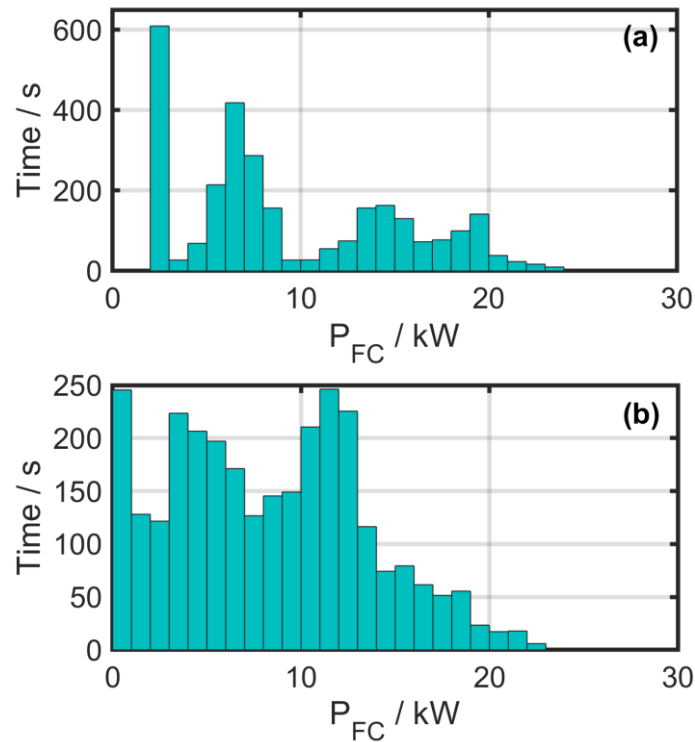


Figure 10: FC power distribution for a) active and b) passive coupling

Figure 11 compares the cost of FC stack caused by the degradation as well as the hydrogen consumption for each considered case under the real driving profile condition. As explained earlier, the degradation cost of the FC stack is due to the idle time, number of start-stops, duration of heavy loading, and the operation time in high power condition. On the one hand, Figure 11 indicates that the FC degradation cost is \$0.1825 and \$0.1961 in active and passive configurations respectively. This result discloses the better performance of the active coupling by almost seven percent in terms of wear and tear in the FC system due to the management of the power between the sources while respecting their defined restrictions. On the other hand,

from Figure 11, it can be seen that the passive connection consumes less hydrogen than the active coupling by virtually 12 percent. This is essentially the result of not having the DC-DC converter electrical losses in the system.

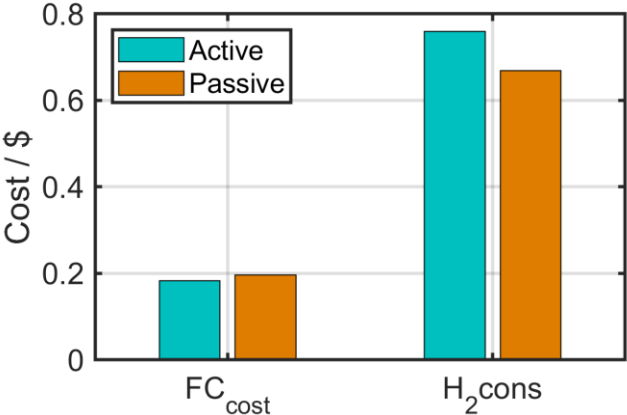


Figure 11: Cost breakdown comparison of active and passive configuration

To scrutinize deeper the pros and cons of having a passive coupling compared to the active one, a more detailed analysis from different perspectives is presented in Table 5.

Table 5: The cost comparison of FC-SC passive and active couplings

Type	Active	Passive
Trip cost	\$ 0.9420	\$ 0.8650
No. Trips per tank	5.36	6.08
No. trips up to EOL of FC	5983	5569
Trip cost up to EOL	\$ 5636	\$ 4817
Capital cost	\$ 3929	\$ 2564
Total cost of the system	\$ 9565	\$ 7381
Total system cost per hour	\$ 1.957	\$ 1.623

According to this table, the trip cost, which is the sum of FC degradation and utilized hydrogen, is less in passive configuration by 8%. Furthermore, the possible number of trips by one tank of hydrogen, calculated by using the total storage capacity of the tank and the hydrogen consumption, is higher in the passive coupling by almost 13.5%. However, the possible number of trips before reaching the EOL of the FC stack is higher in the active coupling by practically 7%, which refers to the faster degradation of the stack in the passive configuration. This table also shows that the total cost of the system, which is composed of capital cost and trip cost up to EOL of the FC stack, is lower in the passive configuration by

22.8%. The last presented result in the table is related to the total cost of operating a passive or active configuration per hour, which is less in the passive coupling by 17%. This cost per hour has been obtained by the division of total cost by the number of hours the FC is able to operate before reaching its EOL. To sum up, Table 5 reveals that a passive coupling, despite of having a shorter operational time in the FC system, leads to a less expensive hourly total cost of the system.

## **5 Conclusions**

This paper performs a comparative study of active and passive FC-SC couplings for the powertrain configuration of e-TESS 3W platform vehicle. In this respect, the size of the components is determined in relation to the requirements of the vehicle in the first place. Afterwards, the performance of the passive configuration is compared with a commonly used active one to spotlight the assets and liabilities of each case. An optimized FLC based on a real driving cycle of the e-TESS 3W platform is used to split the power between the FC stack and SC bank in the active configuration while the passive coupling does not require an EMS for power distribution. In order to investigate the performance of each configuration, an hourly total system cost for the operation of each case is calculated. This cost mainly contains the trip cost, which is composed of the FC degradation and consumed hydrogen costs, and the capital cost of the components. The performed analysis indicates that the hourly cost of the proposed passive connection is 17% less than the studied active configuration. It is worth reminding that the passive configuration causes higher rate of degradation in the FC system compared to the active one. However, this cost is compensated by the other aspects such as lower hydrogen consumption and the capital cost of the system.



## Acknowledgements

This work was supported in part by Grant 950-230863 and 950-230672 from Canada

Research Chairs Program, and in part by Grant RGPIN-2018-06527 and RGPIN-2017-05924

from the Natural Sciences and Engineering Research Council of Canada.

## List of Symbols

$\Delta FC_{deg}$	Voltage degradation of the FC stack / %
$\Delta FC_{add}$	Additional degradation of the FC / %
$\Delta FC_{nat}$	Natural degradation of the FC / %
$CO_2$	Oxygen concentration / mol cm <sup>-3</sup>
$c_p$	Air specific heat capacity / J K <sup>-1</sup>
$C_{SC}$	SC bank capacitance / F
$C_{Trip}$	Cost function / \$
$E_{Nernst}$	Cell reversible voltage / V
$F$	Faraday constant / s A mol <sup>-1</sup>
$F_{air}$	Resistance force against the air / N
$F_{acc}$	Accelerating force / N
$F_{env}$	Traction force resistance / N
$F_{grade}$	Grade related force / N
$F_{roll}$	Rolling resistance force / N
$F_{tr}$	Traction force / N
$g$	Gravity / m sec <sup>-2</sup>
$G_{gb}$	Gearbox transmission ratio
$H_{cons}$	Consumed Hydrogen / kg
$H_{fc}$	Heat transfer coefficient / W K <sup>-1</sup>
$i_{dc/dc}$	Converter current / A
$I_{FC}$	Current of the FC / A
$i_{FC-sys}$	Current of the FC system / A
$i_{SC}$	SC current / A
$i_{ts}$	Electric motor current / A
$k_{tn}$	Empirical coefficient
$MC_{fc}$	Thermal capacity of the FC / kJ K <sup>-1</sup>
$M_{O_2}$	Oxygen molar mass kg mol <sup>-1</sup>
$N_{cell}$	Number of cells
$\eta_{comp}$	Average compressor efficiency
$\eta_{dc/dc}$	Converter efficiency
$\eta_{em}$	Motor average efficiency / %
$\eta_{gb}$	Gearbox transmission efficiency / %
$\eta_{sys}$	Efficiency of the FC system
$\eta_t$	Transmission efficiency / %
$p_{amb}$	Ambient pressure / Pa
$p_{an}$	Pressure in the anode / Pa
$p_{ca}$	Pressure in the cathode / Pa
$P_{comp}$	Consumed power by the compressor / W
$P_e$	Power at maximum speed condition / kW

$P_{fan}$	Consumed power by the FC fan / W
$P_{fc}$	Generated power by the FC / W
$p_{H2}$	Hydrogen partial pressure / Pa
$P_{High}$	FC high power limit / W
$P_{Low}$	FC low power limit / W
$p_{O2}$	Oxygen partial pressure / Pa
$P_{tot}$	Power at maximum acceleration / kW
$P_{ts}$	Transmission power / W
$Q_{conv}$	Convection heat transfer / W
$q_{H2}$	Hydrogen flow / SLPM
$Q_{heat}$	Generated heat in the FC / W
$r_D$	Diode resistance / $\Omega$
$r_{SC}$	SC bank resistance / $\Omega$
$T_{amb}$	Ambient temperature / K
$T_{em}$	Electric machine torque / N m
$T_{em_r}$	Reference torque for electric machine / N m
$T_{fc}$	Stack temperature / K
$U_{act}$	Activation voltage drop / V
$U_{con}$	Concentration voltage drop / V
$U_{fc}$	FC voltage / V
$U_{ohmic}$	Ohmic voltage drop / V
$U_{SC}$	SC voltage / V
$V_{EV}$	vehicle speed / $m\ s^{-1}$
$W_{air}$	Rate of used air
$W_{O2}$	Oxygen consumption rate
$\beta$	Inverse of the limiting current / $A^{-1}$
$\gamma$	Ratio of specific heats of air
$\delta$	Mass factor
$\lambda$	Oxygen excess ratio
$\xi_n$	Parametric coefficients related to ohmic resistance
$\rho_a$	Air density / $kg\ m^{-3}$
$\Upsilon_n$	Exponential coefficients related to activation loss
$\chi_{O2}$	Oxygen mass fraction
$\Omega_m$	Rotor rotation speed / $rad\ s^{-1}$
$k_n$	Degradation coefficient
$t_n$	FC operational time / s

## References

- [1] USDOE Energy Information Administration (EI), Washington, DC (United States). Office of Energy Analysis, **2019**.
- [2] Y. Wu, L. Zhang, *Transportation Research Part D: Transport and Environment* **2017**, *51*, 129-145.
- [3] Z. P. Cano, D. Banham, S. Ye, A. Hintennach, J. Lu, M. Fowler, Z. Chen, *Nature Energy* **2018**, *3*, 279-289.
- [4] B. Hollweck, M. Moullion, M. Christ, G. Kolls, J. Wind, *Fuel Cells* **2018**, *18*, 669-679.
- [5] M. Bodner, A. Schenk, D. Salaberger, M. Rami, C. Hochenauer, V. Hacker, *Fuel Cells* **2017**, *17*, 18-26.
- [6] F. X. Chen, Y. Yu, J. X. Chen, *Fuel Cells* **2017**, *17*, 671-681.
- [7] D. Zhang, C. Cadet, N. Yousfi-Steiner, F. Druart, C. Bérenguer, *Fuel Cells* **2017**, *17*, 268-276.
- [8] X. Zhang, Y. Yang, X. Zhang, L. Guo, H. Liu, *Fuel Cells* **2019**, *19*, 160-168.
- [9] T. Zimmermann, P. Keil, M. Hofmann, M. F. Horsche, S. Pichlmaier, A. Jossen, *Journal of Energy Storage* **2016**, *8*, 78-90.
- [10] R. C. Samsun, C. Krupp, S. Baltzer, B. Gnörich, R. Peters, D. Stolten, *Energy Conversion and Management* **2016**, *127*, 312-323.
- [11] Q. Xun, Y. Liu, E. Holmberg, *Proc. 2018 International Symposium on Power Electronics, Electrical Drives, Automation and Motion (SPEEDAM)*, (Eds. A. Binder, A. Del Pizzo, I. Miki), Amalfi, Italy **2018**, pp. 389-394.
- [12] H. S. Das, C. W. Tan, A. H. M. Yatim, *Renewable and Sustainable Energy Reviews* **2017**, *76*, 268-291.
- [13] J. P. Trovão, M. A. Silva, C. H. Antunes, M. R. Dubois, *Applied Energy* **2017**, *205*, 244-259.

- [14] V. K. Kasimalla, N. S. G., V. Velisala, *International Journal of Energy Research* **2018**, *42*, 4263-4283.
- [15] M. Kandi Dayeni, M. Soleymani, *Clean Technologies and Environmental Policy* **2016**, *18*, 1945-1960.
- [16] R. E. Silva, F. Harel, S. Jemeï, R. Gouriveau, D. Hissel, L. Boulon, K. Agbossou, *Fuel Cells* **2014**, *14*, 894-905.
- [17] C. Turpin, D. Van Laethem, B. Morin, O. Rallières, X. Roboam, O. Verdu, V. Chaudron, *Mathematics and Computers in Simulation* **2017**, *131*, 76-87.
- [18] H. Wang, A. Gaillard, D. Hissel, *Renewable Energy* **2019**, *141*, 124-138.
- [19] S. Ait Hammou Taleb, D. Brown, J. Dillet, P. Guillemet, J. Mainka, O. Crosnier, C. Douard, L. Athouël, T. Brousse, O. Lottin, *Fuel Cells* **2018**, *18*, 299-305.
- [20] K. Gérardin, S. Raël, C. Bonnet, D. Arora, F. Lopicque, *Fuel Cells* **2018**, *18*, 315-325.
- [21] B. Morin, D. Van Laethem, C. Turpin, O. Rallières, S. Astier, A. Jaafar, O. Verdu, M. Plantevin, V. Chaudron, *Fuel Cells* **2014**, *14*, 500-507.
- [22] R. Shimoi, Y. Ono, *WIPO*, *WO2005107360*, **2005**.
- [23] D. Arora, K. Gérardin, S. Raël, C. Bonnet, F. Lopicque, *Journal of Applied Electrochemistry* **2018**.
- [24] 2.7V 650-3000F ultracapacitor, can be found under <https://www.maxwell.com>, **2013**.
- [25] P. Pei, Q. Chang, T. Tang, *International Journal of Hydrogen Energy* **2008**, *33*, 3829-3836.
- [26] H. Zhao, A. F. Burke, *Fuel Cells* **2010**, *10*, 879-896.
- [27] B. Wu, M. A. Parkes, V. Yufit, L. De Benedetti, S. Veismann, C. Wirsching, F. Vesper, R. F. Martinez-Botas, A. J. Marquis, G. J. Offer, N. P. Brandon, *International Journal of Hydrogen Energy* **2014**, *39*, 7885-7896.
- [28] J. P. F. Trovão, M. R. Dubois, M. Roux, E. Menard, A. Desrochers, *Proc. 2015 IEEE Vehicle Power and Propulsion Conference (VPPC)*, Montreal, Quebec, **2015**, pp. 1-6.

- [29] J. P. F. Trovão, M. Roux, É. Ménard, M. R. Dubois, *IEEE Transactions on Vehicular Technology* **2017**, *66*, 5540-5550.
- [30] A. S. Mohammadi, J. P. Trovão, M. R. Dubois, *IET Electrical Systems in Transportation* **2018**, *8*, 12-19.
- [31] G. Wenzhong, *IEEE Transactions on Vehicular Technology* **2005**, *54*, 846-855.
- [32] R. Abousleiman, O. Rawashdeh, *2015 IEEE Transportation Electrification Conference and Expo (ITEC)*, **2015**, pp. 1-5.
- [33] C. Mi, M. A. Masrur, *Hybrid electric vehicles: principles and applications with practical perspectives*, John Wiley & Sons, **2017**.
- [34] FCvelocity®-9SSL Product Manual and Integration Guide, can be found under [www.ballard.com](http://www.ballard.com), **2017**.
- [35] V. Liso, M. P. Nielsen, S. K. Kær, H. H. Mortensen, *International Journal of Hydrogen Energy* **2014**, *39*, 8410-8420.
- [36] C. H. Choi, S. Yu, I.-S. Han, B.-K. Kho, D.-G. Kang, H. Y. Lee, M.-S. Seo, J.-W. Kong, G. Kim, J.-W. Ahn, S.-K. Park, D.-W. Jang, J. H. Lee, M. Kim, *International Journal of Hydrogen Energy* **2016**, *41*, 3591-3599.
- [37] Fuel Cell Technologies Office Multi-Year Research, Development, and Demonstration Plan - Hydrogen Storage, can be found under [www.energy.gov](http://www.energy.gov), **2015**.
- [38] A. Bouscayrol, in *Systemic Design Methodologies for Electrical Energy Systems* (Ed. X. Roboam), ISTE, **2012**, pp. 89.
- [39] L. Boulon, D. Hissel, A. Bouscayrol, M. Pera, *IEEE Transactions on Industrial Electronics* **2010**, *57*, 1882-1891.
- [40] M. Kandidayeni, A. Macias, A. A. Amamou, L. Boulon, S. Kelouwani, *Fuel Cells* **2018**, *18*, 347-358.
- [41] P. S. Oruganti, Q. Ahmed, D. Jung, *Proc. WCX World Congress Experience*, Michigan, U.S.A., **2018**.

- [42] X. Zhao, Y. Li, Z. Liu, Q. Li, W. Chen, *International Journal of Hydrogen Energy* **2015**, *40*, 3048-3056.
- [43] J. M. Campbell, *Gas conditioning and processing Volume 2: The Equipment modules*, PetroSkills, U.S.A., **2014**, pp. 197.
- [44] L. Zubieta, R. Bonert, *IEEE Transactions on Industry Applications* **2000**, *36*, 199-205.
- [45] Y. Wang, S. J. Moura, S. G. Advani, A. K. Prasad, *International Journal of Hydrogen Energy* **2019**.
- [46] Z. Hu, J. Li, L. Xu, Z. Song, C. Fang, M. Ouyang, G. Dou, G. Kou, *Energy Conversion and Management* **2016**, *129*, 108-121.
- [47] K. Song, H. Chen, P. Wen, T. Zhang, B. Zhang, T. Zhang, *Electrochimica Acta* **2018**, *292*, 960-973.
- [48] Fuel Cell Technologies Office Multi-Year Research, Development, and Demonstration Plan - Fuel Cells, can be found under [www.energy.gov](http://www.energy.gov), **2015**.
- [49] R. Zhang, J. Tao, *IEEE Transactions on Fuzzy Systems* **2018**, *26*, 1833-1843.
- [50] R. Zhang, J. Tao, H. Zhou, *IEEE Transactions on Fuzzy Systems* **2019**, *27*, 45-57.
- [51] Fuel Cell Technologies Office Multi-Year Research, Development, and Demonstration Plan - Hydrogen Production, can be found under [www.energy.gov](http://www.energy.gov), **2015**.
- [52] Z. Song, J. Li, J. Hou, H. Hofmann, M. Ouyang, J. Du, *Energy* **2018**, *154*, 433-441.
- [53] Electrical and Electronics Technical Team Roadmap, can be found under [www.energy.gov](http://www.energy.gov), **2017**.